Hindawi
Journal of Nanomaterials
Volume 2021, Article ID 3743876, 17 pages
https://doi.org/10.1155/2021/3743876

Research Article

Impact of Ramped Concentration and Temperature on MHD Casson Nanofluid Flow through a Vertical Channel

Kashif Sadiq,[1] Imran Siddique,[1] Rifaqat Ali,[2] and Fahd Jarad[3,4]

[1]*Department of Mathematics, University of Management and Technology, Lahore 54770, Pakistan*
[2]*Department of Mathematics, College of Science and Arts, King Khalid University, Muhayil, Abha 61413, Saudi Arabia*
[3]*Department of Mathematics, Cankaya University, Etimesgut, Ankara, Turkey*
[4]*Department of Medical Research, China Medical University Hospital, China Medical University, Taichung, Taiwan*

Correspondence should be addressed to Imran Siddique; imransmsrazi@gmail.com and Fahd Jarad; fahd@cankaya.edu.tr

Received 10 September 2021; Accepted 8 October 2021; Published 31 October 2021

Academic Editor: Taza Gul

The mass and heat transport of Casson nanofluid flow in a channel under the influence of the magnetic field, heat generation, chemical reaction, ramped concentration, and ramped temperature is studied. Nanoparticles of copper (Cu) are inserted in sodium alginate (SA) to make nanofluid. The definition of time-fractional Caputo derivative is applied to have the fractional model. The analytical results of concentration, temperature, velocity, skin friction, Sherwood numbers, and Nusselt numbers for ramped and isothermal boundary conditions are obtained in the form of summation after applying the Laplace inverse transform. The effects of the fractional parameter (ξ) and physical parameters are depicted graphically. For higher values of ξ the velocity, concentration and temperature reduce. The fractional model is a better choice to control velocity, concentration, and temperature profiles. The energy enhances by increasing volume fraction (ϕ), whereas mass and flow of nanofluid reduce. The Sherwood and Nusselt numbers for both isothermal and ramped conditions increase by increasing ϕ. Ramped conditions can control the flow, mass, and heat of the nanofluid.

1. Introduction

Non-Newtonian fluids have attracted several scientists and researchers due to their industrial applications such as cosmetics, synthetic lubricants, clay coating, certain oils, paint, synthetic lubricants, certain oils, biological fluids, pharmaceuticals, and drilling muds. The flow features of non-Newtonian cannot be defined briefly by the Navier-Stokes equation due to the complex formulation of the problem. Thus, according to qualities, different models of non-Newtonian fluids are categorized such as Seely, Bulky, Jeffry, Eyring-Powell, Oldroyd-B, Burger, Oldroyd-A, Carreau, Maxwell, and Casson. For the expectancy of flow tendency of balanced pigment oil, Casson [1] introduced the model of Casson fluid in 1959. Casson fluid is a shear-thinning fluid with endless and zero viscosity at zero and infinite shear, respectively [2]. Tomato sauce, jelly, human blood, soup, and honey are examples of Casson fluids.

Many researchers and scientists are investigating nanofluids due to their common uses in industrial and engineering fields. They have revealed the significant thermal characteristics and ways to boost the thermal conductivity of nanofluids. The addition of nanofluids and biotechnological apparatus may give proficient applications in agriculture, pharmaceuticals, and biosensors. Several nanomaterials are used in biotechnology, for instance, nanowires, nanostructures, nanoparticles, and nanofibers. The significance of microfluidics and nanofluids is unquestionable in biomedical devices. MHD nanofluids have magnetic and liquid characteristics; it has several applications, for instance, optical controls, modulators, and adjustable fiber filters. Magnetic nanoparticles are very significant for the treatment of cancer in medicine. The researchers are using nanofluids to improve the efficiency of and thermal conductivity of conventional fluids [3–6]. Zari et al. [7] numerically investigated Casson nanofluid flow on an

inclined plate with double stratification. Ali et al. [8] discussed the numerical results of Carreau flow of Casson nanofluid with magnetohydrodynamics. Shafiq et al. [9] analyzed Casson nanofluid flow on a rotating disk.

Daily life problems frequently have arbitrary wall conditions. It is practical to study such problems in which wall temperature changes step-wise. Researchers are making a lot of efforts to investigate such problems. The flow of heat in fluids demonstrates a vital role in extensive engineering and industrial procedures, such as nuclear operations, gas turbines, processes of heating and cooling, scheming of devices, and supervision of high-tech thermal systems. The studies of the flow of MHD nanofluid with ramped concentration and temperature conditions in the literature currently are not discussed analytically in detail due to its complicated relations. Hayday et al. [10], Schetz [11], and Malhotra et al. [12] have established the idea of ramped temperature. The most significant use of ramped heat is to raze cancer cells during thermal therapy. Ramped conditions help to control the temperature rise caused by natural conditions [13]. The impact of ramped heating on an incompressible visually thin fluid flow above a plate was examined by Das et al. [14]. Nandkeolyar et al. [15] evaluated and compared MHD natural convection flow and diverse movements of the plate having uniform velocity, periodic acceleration, and single acceleration due to ramped and constant boundary conditions. Seth et al. [16–19] investigated mass and heat transport in the existence of various parameters like chemical reaction, heat absorption, Darcy's law, thermal radiation, porous medium, and Hall current with ramped concentration and temperature on a vertical plate. Zin et al. [20] analyzed the effects of ramped temperature, thermal radiation, and magnetic field on the natural convection Jeffrey fluid flow.

Narahari [21] investigated the effects of ramped heating and thermal radiation through a channel. Khalid et al. [22] compared the ramped and isothermal boundary conditions of convective nanofluid flow. Mahanthesh et al. [23] evaluated the analytical results of nanofluid flow over a plate in the existence of heat generation and magnetic field. Jha and Gambo [24] examined mass and heat transport of transient free convective flow affected by the Dufour and Soret effect through a channel with ramped temperature and concentration. Arif et al. [25] studied fractionalized Casson fluid flow on a plate with ramped concentration and temperature. Anwer et al. [26] discussed MHD Oldroyd-B convective flow of nanofluid with ramped velocity and ramped temperature. The MHD Casson nanofluid flow with ramped concentration and temperature through a channel is not investigated in literature yet.

The mathematical models described by fractional differential equations are useful because such models include the memory effects, therefore offering more information regarding the complex diffusive processes. Also, for some experiments, the adequate fractional model could be chosen that gives the best agreement between analytical results and those experimental. Therefore, researchers are using fractional models instead of classical ones to meet the growing demand of modern technology. Fractional calculus is very effective in diffusion, electrochemistry, relaxation processes, and viscoelasticity. Fractional models help to understand memory and hereditary properties that were not possible with integral models. Fractional models are applicable in modern sciences like mathematical biology, applied sciences, physics, and fractals. Various definitions of fractional derivatives are available in the literature. Riemann-Liouville defined Caputo derivative [27] for physical problems like viscoelasticity, electrohysteresis, and damage and fatigue. Riemann-Liouville [28] used fractional derivatives to solve complex problems. For example, the nonzero result fractional derivative of constant.

Motivated by the above literature focus of this work is to scrutinize the results of chemical reaction, heat generation, and magnetic force with ramped concentration and temperature unsteady flow of Casson nanofluid. The nanofluid is prepared by adding nanoparticles of Cu into SA. The analytical results of velocity, skin friction, temperature, Nusselt numbers, concentration, and Sherwood numbers for isothermal and ramped wall boundary conditions are calculated by using the Laplace transform. The significant results are illustrated graphically and discussed in detail.

2. Mathematical Model

Consider the Casson nanofluid flow through a vertical channel with heat and mass transport under the effect of magnetic force, chemical reaction, and heat generation. The nanoparticles of Cu are suspended uniformly into SA. Initially, the walls of the channel and nanofluid are at rest at fixed temperature $\widetilde{T_l}$ and concentration $\widetilde{C_l}$ at $\tilde{t} = 0$. At time $\tilde{t} = 0^+$, the concentration and temperature of the left wall rise momentarily to $\widetilde{C_l} + (\widetilde{C_0} - \widetilde{C_l})\tilde{t}/\widetilde{t_0}$ and $\widetilde{T_l} + (\widetilde{T_0} - \widetilde{T_l})\tilde{t}/\widetilde{t_0}$, respectively, for $0 < \tilde{t} < \widetilde{t_0}$; the concentration and temperature are maintained at C_0 and T_0 when $\tilde{t} > \widetilde{t_0}$. The initial concentration $\widetilde{C_l}$ and temperature $\widetilde{T_l}$ will remain unchanged on the right wall at $\tilde{y} = l$. A constant magnetic force B_0 is applied perpendicularly on the left wall externally (see Figure 1).

Thermophysical characteristics SA and Cu are assumed constant and shown in Table 1. The slippage between SA and Cu is negligible due to thermal equilibrium. The addition of nanoparticles of Cu in SA makes the fluid thick and reduces the flow.

By the above assumptions, the governing equations of unsteady flow are [31, 32]

$$\rho_{nf}\frac{\partial\tilde{u}(\tilde{y},\tilde{t})}{\partial\tilde{t}} = \mu_{nf}\left(1+\frac{1}{\gamma}\right)\frac{\partial^2\tilde{u}(\tilde{y},\tilde{t})}{\partial\tilde{y}^2} + g(\rho\beta_C)_{nf}\left(\tilde{C}(\tilde{y},\tilde{t}) - \widetilde{C_l}\right) + g(\rho\beta_T)_{nf}\left(\tilde{T}(\tilde{y},\tilde{t}) - \widetilde{T_l}\right) - \sigma_{nf}{B_0}^2\tilde{u}(\tilde{y},\tilde{t}), \tag{1}$$

$$\left(\rho c_p\right)_{nf}\frac{\partial\tilde{T}(\tilde{y},\tilde{t})}{\partial\tilde{t}} = k_{nf}\frac{\partial^2\tilde{T}(\tilde{y},\tilde{t})}{\partial\tilde{y}^2} + Q_0\left(\tilde{T}(\tilde{y},\tilde{t}) - \widetilde{T_l}\right), \tag{2}$$

$$\frac{\partial\tilde{C}(\tilde{y},\tilde{t})}{\partial\tilde{t}} = D_{nf}\frac{\partial^2\tilde{C}}{\partial\tilde{y}^2} - K_C\left(\tilde{C}(\tilde{y},\tilde{t}) - \widetilde{C_l}\right), \tag{3}$$

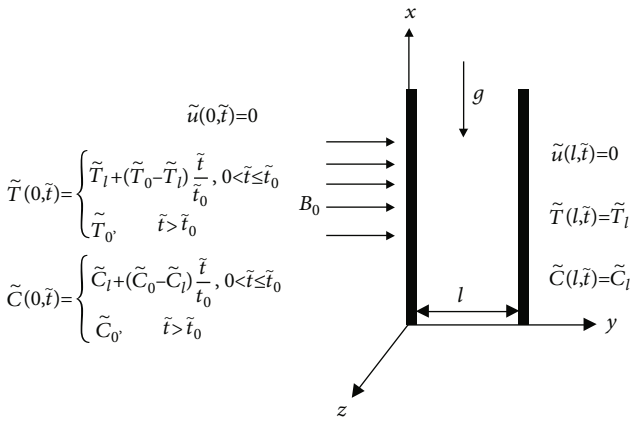

Figure 1: Flow geometry.

with corresponding initial and boundary conditions

$$\tilde{u}(\tilde{y},0)=0, \tag{4}$$

$$\tilde{T}(\tilde{y},0)=\widetilde{T_l}, \tag{5}$$

$$\tilde{C}(\tilde{y},0)=\widetilde{C_l}, \tag{6}$$

$$0\le\tilde{y}\le l, \tag{7}$$

$$\tilde{u}(0,\tilde{t})=0,\ \tilde{T}(0,\tilde{t})=\begin{cases}\widetilde{T_l}+\left(\widetilde{T_0}-\widetilde{T_l}\right)\dfrac{\tilde{t}}{\widetilde{t_0}}, & 0<\tilde{t}\le\widetilde{t_0},\\ \widetilde{T_0}, & \tilde{t}>\widetilde{t_0},\end{cases} \tag{8}$$

$$\tilde{C}(0,\tilde{t})=\begin{cases}\widetilde{C_l}+\left(\widetilde{C_0}-\widetilde{C_l}\right)\dfrac{\tilde{t}}{t_0}, & 0<\tilde{t}\le\widetilde{t_0},\\ \widetilde{C_0}, & \tilde{t}>\widetilde{t_0},\end{cases} \tag{9}$$

$$\tilde{u}(l,\tilde{t})=0, \tag{10}$$

$$\tilde{T}(l,\tilde{t})=\widetilde{T_l}, \tag{11}$$

$$\tilde{C}(l,\tilde{t})=\widetilde{C_l}. \tag{12}$$

The expressions of nanofluid are defined by [33, 34].

$$\frac{\mu_{nf}}{\mu_f}=\frac{1}{(1-\phi)^{2.5}},$$

$$\frac{\rho_{nf}}{\rho_f}=(1-\phi)+\phi\frac{\rho_s}{\rho_f},$$

$$\frac{(\rho c_p)_{nf}}{(\rho c_p)_f}=(1-\phi)+\phi\frac{(\rho c_p)_s}{(\rho c_p)_f},$$

$$\frac{(\rho\beta_T)_{nf}}{(\rho\beta_T)_f}=(1-\phi)+\phi\frac{(\rho\beta_T)_s}{(\rho\beta_T)_f},$$

$$\frac{(\rho\beta_C)_{nf}}{(\rho\beta_C)_f}=(1-\phi)+\phi\frac{(\rho\beta_C)_s}{(\rho\beta_C)_f},$$

$$D_{nf}=(1-\phi)D_f,$$

$$\frac{\sigma_{nf}}{\sigma_f}=\left[1+\frac{3\left(\left(\sigma_s/\sigma_f\right)-1\right)\phi}{\left(\left(\sigma_s/\sigma_f\right)+2\right)-\left(\left(\sigma_s/\sigma_f\right)-1\right)\phi}\right],$$

$$\frac{k_{nf}}{k_f}=\left[\frac{k_s+2k_f-2\phi\left(k_f-k_s\right)}{k_s+2k_f+\phi\left(k_f-k_s\right)}\right]. \tag{13}$$

Introducing the dimensionless parameters, functions, and variables,

$$u=\frac{\tilde{u}}{U_0}, \tag{14}$$

$$t=\frac{\tilde{t}}{\widetilde{t_0}},$$

$$\widetilde{t_0}=\frac{l^2}{\nu_f},$$

$$y=\frac{\tilde{y}}{l},$$

$$\theta=\frac{\tilde{T}-\widetilde{T_l}}{\widetilde{T_0}-\widetilde{T_l}},$$

$$C=\frac{\tilde{C}-\widetilde{C_l}}{\widetilde{C_0}-\widetilde{C_l}},$$

$$\psi_1=\frac{1}{(1-\phi)^{2.5}}\frac{\rho_f}{\rho_{nf}}\left(1+\frac{1}{\beta}\right),$$

$$\psi_2=Gm\frac{(\beta_C)_{nf}}{(\beta_C)_f},$$

$$\psi_3=Gr\frac{(\beta_T)_{nf}}{(\beta_T)_f},$$

$$\psi_4=M\frac{\sigma_{nf}\rho_f}{\sigma_f\rho_{nf}},$$

$$\psi_5=\frac{1}{\mathrm{Pr}}\frac{k_{nf}\left(\rho c_p\right)_f}{k_f\left(\rho c_p\right)_{nf}},$$

$$\psi_6=Q\frac{\left(\rho c_p\right)_f}{\left(\rho c_p\right)_{nf}},$$

$$\psi_7=\frac{1-\phi}{Sc},$$

$$\psi_8=K=\frac{K_C l^2}{\nu_f},$$

$$Gm=\frac{g(\beta_C)_f(C_0-C_l)d^2}{U_0\nu_f},$$

Table 1: Thermophysical characteristics of Cu and SA [29, 30].

Material	ρ (kg/m^3)	C_p (J/kg·K)	k (W/m·K)	$\beta \times 10^5$ (K^{-1})	σ (Ωm)$^{-1}$
Sodium alginate $C_6H_9NaO_7$(SA)	989	4175	0.6376	0.99	5.5×10^{-6}
Copper (Cu)	8933	385	401	1.67	59.6×10^6

$$Gr = \frac{g(\beta_T)_f (T_0 - T_l) d^2}{U_0 \nu_f},$$
$$M = \frac{\sigma_f {B_0}^2 l^2}{\mu_f},$$
$$Q = \frac{Q_0 l^2}{(\rho c_p)_f \nu_f},$$
$$\Pr = \frac{(\rho c_p)_f \nu_f}{k_f}, Sc = \frac{\nu_f}{D_f}. \quad (15)$$

By substituting equation (15) to equations (1)–(12), we get

$$\frac{\partial u(y,t)}{\partial t} = \psi_1 \frac{\partial^2 u(y,t)}{\partial y^2} + \psi_2 C(y,t) + \psi_3 \theta(y,t) - \psi_4 u(y,t), \quad (16)$$

$$\frac{\partial \theta(y,t)}{\partial t} = \psi_5 \frac{\partial^2 \theta(y,t)}{\partial y^2} + \psi_6 \theta(y,t), \quad (17)$$

$$\frac{\partial C(y,t)}{\partial t} = \psi_7 \frac{\partial^2 C(y,t)}{\partial y^2} - \psi_8 C(y,t). \quad (18)$$

$$u(y,0) = 0, \theta(y,0) = 0, C(y,0) = 0, \quad 0 \le y \le 1, \quad (19)$$

$$u(0,t) = 0,$$
$$\theta(0,t) = C(0,t) = \begin{cases} t, & 0 < t \le 1, \\ 1, & t > 1, \end{cases} = H(t)t - H(t-1)(t-1), \quad (20)$$

$$u(1,t) = 0,$$
$$\theta(1,t) = 0, \quad (21)$$
$$C(1,t) = 0.$$

The researchers used Caputo time-fractional derivatives of order ξ to develop fractional models in equations (16)–(18).

$$D_t^{\xi} u(y,t) = \psi_1 \frac{\partial^2 u(y,t)}{\partial y^2} + \psi_2 C(y,t) + \psi_3 \theta(y,t) - \psi_4 u(y,t), \quad (22)$$

$$D_t^{\xi} \theta(y,t) = \psi_5 \frac{\partial^2 \theta(y,t)}{\partial y^2} + \psi_6 \theta(y,t), \quad (23)$$

$$D_t^{\xi} C(y,t) = \psi_7 \frac{\partial^2 C(y,t)}{\partial y^2} - \psi_8 C(y,t). \quad (24)$$

Where $D_t^{\xi} u(y,t)$ represents the time-fractional Caputo derivative,

$$D_t^{\xi} u(\eta,\tau) = \begin{cases} \frac{1}{\Gamma(1-\xi)} \int_0^{\tau} (\tau - w)^{\xi} \frac{\partial u(\eta,w)}{\partial w} dw, & 0 \le \xi < 1; \\ \frac{\partial u(\eta,\tau)}{\partial \tau}, & \xi = 1. \end{cases} \quad (25)$$

3. Solution of the Problem

3.1. Concentration. Applying Laplace transform (LT) to equations (24), $(20)_3$, and $(21)_3$ and using $(19)_3$, we obtain

$$\psi_7 \frac{\partial^2 \bar{C}(y,s)}{\partial y^2} - \left(s^{\xi} + \psi_8\right) \bar{C}(y,s) = 0, \quad (26)$$

$$\bar{C}(0,s) = s^{-2}(1 - e^{-s}),$$
$$\bar{C}(1,s) = 0. \quad (27)$$

The solution of equation (26) subject to equation (27) gives

$$\bar{C}(y,s) = (1 - e^{-s}) \frac{\sinh\left[(1-y)\sqrt{(s^{\xi} + \psi_8)/\psi_7}\right]}{s^2 \sinh\left[\sqrt{(s^{\xi} + \psi_8)/\psi_7}\right]}. \quad (28)$$

This expression can be written as

$$\bar{C}(y,s) = (1 - e^{-s}) \left(\frac{1}{s^{2-\xi}} + \frac{\psi_8}{s^2}\right) \cdot \sum_{k=0}^{\infty} \left[\frac{e^{-(2k+y)\sqrt{(s^{\xi}+\psi_8)/\psi_7}}}{s^{\xi} + \psi_8} - \frac{e^{-(2k+2-y)\sqrt{(s^{\xi}+\psi_8)/\psi_7}}}{s^{\xi} + \psi_8}\right]. \quad (29)$$

Taking inverse LT of equation (29), we get

$$C(y,t) = C_0(y,t) - H(t-1) C_0(y,t-1), \quad (30)$$

where

$$C_0(y,t) = \sum_{k=0}^{\infty} \int_0^t \left(\frac{(t-p)^{1-\xi}}{\Gamma(2-\xi)} + \psi_8 (t-p)\right) \cdot \left(g\left(\frac{2k+y}{\sqrt{\psi_7}}, \psi_8, p\right) - g\left(\frac{2k+2-y}{\sqrt{\psi_7}}, \psi_8, p\right)\right) dp,$$
$$g(a,b,p) = \int_0^{\infty} e^{-bu} \operatorname{erfc}\left(\frac{a}{2\sqrt{u}}\right) \frac{1}{p} \Phi\left(0, -\xi, -up^{-\xi}\right) du. \quad (31)$$

3.2. Temperature Distribution. Applying LT to equations (23), $(20)_2$, and $(21)_2$ and using $(19)_2$, we obtain

$$\psi_5 \frac{\partial^2 \overline{\theta}(y,s)}{\partial y^2} - \left(s^{\xi} - \psi_6\right)\overline{\theta}(y,s) = 0, \tag{32}$$

$$\begin{aligned} \overline{\theta}(0,s) &= s^{-2}(1-e^{-s}), \\ \overline{\theta}(1,s) &= 0. \end{aligned} \tag{33}$$

The solution of equation (32) subject to equation (33) gives

$$\bar{\theta}(y,s) = (1-e^{-s})\frac{\sinh\left[(1-y)\sqrt{(s^{\xi}-\psi_6)/\psi_5}\right]}{s^2\sinh\left[\sqrt{(s^{\xi}-\psi_6)/\psi_5}\right]}. \tag{34}$$

This expression can be written as

$$\begin{aligned} \bar{\theta}(y,s) = (1-e^{-s})&\left(\frac{1}{s^{2-\xi}} - \frac{\psi_6}{s^2}\right) \\ &\cdot \sum_{k=0}^{\infty}\left[\frac{e^{-(2k+y)\sqrt{(s^{\xi}-\psi_6)/\psi_5}}}{s^{\xi}-\psi_6} - \frac{e^{-(2k+2-y)\sqrt{(s^{\xi}-\psi_6)/\psi_5}}}{s^{\xi}-\psi_6}\right]. \end{aligned} \tag{35}$$

Taking inverse LT of equation (35), we get

$$\theta(y,t) = \theta_0(y,t) - H(t-1)\theta_0(y,t-1), \tag{36}$$

where

$$\begin{aligned} \theta_0(y,t) = \sum_{k=0}^{\infty}\int_0^t &\left(\frac{(t-p)^{1-\xi}}{\Gamma(2-\xi)} - \psi_6(t-p)\right) \\ &\cdot \left(g\left(\frac{2k+y}{\sqrt{\psi_5}}, -\psi_6, p\right) - g\left(\frac{2k+2-y}{\sqrt{\psi_5}}, -\psi_6, p\right)\right)dp. \end{aligned} \tag{37}$$

3.3. Velocity Field. Applying LT to equations (22), $(20)_1$, and $(21)_1$ and using $(19)_1$, we obtain

$$\psi_1 \frac{\partial^2 \bar{u}(y,s)}{\partial y^2} - \left(s^{\xi} + \psi_4\right)\bar{u}(y,s) = -\psi_2\bar{C}(y,s) - \psi_3\overline{\theta}(y,s), \tag{38}$$

$$\begin{aligned} \bar{u}(0,s) &= 0, \\ \bar{u}(1,s) &= 0. \end{aligned} \tag{39}$$

The solution of equation (38) subject to equation (39) gives

$$\begin{aligned} \bar{u}(y,s) = (1-e^{-s})&\left(\frac{a_1}{s^{\xi}+a_2} + \frac{a_3}{s^{\xi}+a_4}\right)\frac{\sinh\left[(1-y)\sqrt{(s^{\xi}+\psi_4)/\psi_1}\right]}{s^2\sinh\left[\sqrt{(s^{\xi}+\psi_4)/\psi_5}\right]} \\ &- (1-e^{-s})\left(\frac{a_1}{s^{\xi}+a_2}\right)\frac{\sinh\left[(1-y)\sqrt{(s^{\xi}+\psi_8)/\psi_7}\right]}{s^2\sinh\left[\sqrt{(s^{\xi}+\psi_8)/\psi_7}\right]} \\ &- (1-e^{-s})\left(\frac{a_3}{s^{\xi}+a_4}\right)\frac{\sinh\left[(1-y)\sqrt{(s^{\xi}+\psi_6)/\psi_5}\right]}{s^2\sinh\left[\sqrt{(s^{\xi}+\psi_6)/\psi_5}\right]}. \end{aligned} \tag{40}$$

This expression can be as

$$\begin{aligned} \bar{u}(y,s) = (1-e^{-s})&\left[\left(\frac{a_1+a_3}{s^2} + \frac{a_1(\psi_4-a_2)}{s^2\left(s^{\xi}+a_2\right)} + \frac{a_3(\psi_4-a_4)}{s^2\left(s^{\xi}+a_4\right)}\right)\right. \\ &\cdot \sum_{k=0}^{\infty}\left(\frac{e^{-(2k+y)\sqrt{(s^{\xi}+\psi_4)/\psi_1}}}{s^{\xi}+\psi_4} - \frac{e^{-(2k+2-y)\sqrt{(s^{\xi}+\psi_4)/\psi_1}}}{s^{\xi}+\psi_4}\right) \\ &- \left(\frac{a_1}{s^2} + \frac{a_1(\psi_8-a_2)}{s^2\left(s^{\xi}+a_2\right)}\right)\sum_{k=0}^{\infty}\left(\frac{e^{-(2k+y)\sqrt{(s^{\xi}+\psi_8)/\psi_7}}}{s^{\xi}+\psi_8}\right. \\ &\left. - \frac{e^{-(2k+2-y)\sqrt{(s^{\xi}+\psi_8)/\psi_7}}}{s^{\xi}+\psi_8}\right) - \left(\frac{a_3}{s^2} - \frac{a_3(\psi_6+a_4)}{s^2\left(s^{\xi}+a_4\right)}\right) \\ &\left.\cdot \sum_{k=0}^{\infty}\left(\frac{e^{-(2k+y)\sqrt{(s^{\xi}+\psi_6)/\psi_5}}}{s^{\xi}-\psi_6} - \frac{e^{-(2k+2-y)\sqrt{(s^{\xi}+\psi_6)/\psi_5}}}{s^{\xi}-\psi_6}\right)\right]. \end{aligned} \tag{41}$$

Taking inverse LT of equation (41), we get

$$u(y,t) = u_0(y,t) - H(t-1)u_0(y,t-1), \tag{42}$$

where

$$\begin{aligned} u_0(y,t) = \sum_{k=0}^{\infty}\int_0^t &((a_1+a_3)(t-p) + a_1(\psi_4-a_2)f_1(t-p) \\ &+ a_3(\psi_4-a_4)f_2(t-p))\left(g\left(\frac{2k+y}{\sqrt{\psi_1}}, \psi_4, p\right)\right. \\ &\left. - g\left(\frac{2k+2-y}{\sqrt{\psi_1}}, \psi_4, p\right)\right)dp - \sum_{k=0}^{\infty}\int_0^t (a_1(t-p) \\ &+ a_1(\psi_8-a_2)f_1(t-p))\left(g\left(\frac{2k+y}{\sqrt{\psi_7}}, \psi_8, p\right)\right. \\ &\left. - g\left(\frac{2k+2-y}{\sqrt{\psi_7}}, \psi_8, p\right)\right)dp - \sum_{k=0}^{\infty}\int_0^t (a_3(t-p) \\ &- a_3(\psi_6+a_4)f_2(t-p))\left(g\left(\frac{2k+y}{\sqrt{\psi_5}}, -\psi_6, p\right)\right. \\ &\left. - g\left(\frac{2k+2-y}{\sqrt{\psi_5}}, -\psi_6, p\right)\right)dp, \end{aligned}$$

$$f_1(t) = \int_0^t w^{\xi} E_{\xi,\xi+1}\left(-a_2 w^{\xi}\right) dw,$$

$$f_2(t) = \int_0^t w^{\xi} E_{\xi,\xi+1}\left(-a_4 w^{\xi}\right) dw. \tag{43}$$

3.4. Sherwood Numbers, Skin Friction, and Nusselt Numbers. Skin friction at $y = 0$ is defined as

$$C_{f_0} = -\frac{\mu_{nf}}{\mu_f}\frac{\partial u(y,t)}{\partial y}\bigg|_{y=0} = -(1-\phi)^{-2.5} L^{-1}\left\{\frac{\partial \bar{u}(y,s)}{\partial y}\bigg|_{y=0}\right\}. \tag{44}$$

By using equation (41) in equation (44),

$$C_{f_0} = \frac{1}{(1-\phi)^{2.5}}\left[u_1(t) - H(t-1)u_1(t-1)\right], \tag{45}$$

where

$$\begin{aligned} u_1(t) = {} & \frac{1}{\sqrt{\psi_1}}\sum_{k=0}^{\infty}\int_0^t ((a_1+a_3)(t-p) + a_1(\psi_4 - a_2)f_1(t-p) \\ & + a_3(\psi_4 - a_4)f_2(t-p))\left(L'\left(\frac{k}{\sqrt{\psi_1}}, \psi_4, p\right)\right. \\ & \left. + L'\left(\frac{k+1}{\sqrt{\psi_1}}, \psi_4, p\right)\right) dp - \frac{1}{\sqrt{\psi_7}}\sum_{k=0}^{\infty}\int_0^t (a_1(t-p) \\ & + a_1(\psi_8 - a_2)f_1(t-p))\left(L'\left(\frac{k}{\sqrt{\psi_7}}, \psi_8, p\right)\right. \\ & \left. + L'\left(\frac{k+1}{\sqrt{\psi_7}}, \psi_8, p\right)\right) dp - \frac{1}{\sqrt{\psi_5}}\sum_{k=0}^{\infty}\int_0^t (a_3(t-p) \\ & - a_3(\psi_6 + a_4)f_2(t-p))\left(L'\left(\frac{k}{\sqrt{\psi_5}}, -\psi_6, p\right)\right. \\ & \left. + L'\left(\frac{k+1}{\sqrt{\psi_5}}, -\psi_6, p\right)\right) dp, \end{aligned}$$

$$L'(a,b,p) = \int_0^{\infty} \frac{1}{\sqrt{\pi w}} e^{-\left(\left(a^2/4w\right)+bw\right)} \frac{1}{p}\Phi\left(0, -\xi, -wp^{-\xi}\right) dw. \tag{46}$$

Skin friction at $y = 1$ is defined as

$$C_{f_1} = -\frac{\mu_{nf}}{\mu_f}\frac{\partial u(y,t)}{\partial y}\bigg|_{y=1} = -(1-\phi)^{-2.5} L^{-1}\left\{\frac{\partial \bar{u}(y,s)}{\partial y}\bigg|_{y=1}\right\}. \tag{47}$$

By using equation (41) in equation (47),

$$C_{f_1} = \frac{1}{(1-\phi)^{2.5}}\left[u_2(t) - H(t-1)u_2(t-1)\right], \tag{48}$$

where

$$\begin{aligned} u_2(t) = {} & \frac{1}{\sqrt{\psi_1}}\sum_{k=0}^{\infty}\int_0^t ((a_1+a_3)(t-p) + a_1(\psi_4 - a_2)f_1(t-p) \\ & + a_3(\psi_4 - a_4)f_2(t-p))\left(2L'\left(\frac{2k+1}{\sqrt{\psi_1}}, \psi_4, p\right)\right) dp \\ & - \frac{1}{\sqrt{\psi_7}}\sum_{k=0}^{\infty}\int_0^t (a_1(t-p) + a_1(\psi_8 - a_2)f_1(t-p)) \\ & \cdot \left(2L'\left(\frac{2k+1}{\sqrt{\psi_7}}, \psi_8, p\right)\right) dp - \frac{1}{\sqrt{\psi_5}} \\ & \cdot \sum_{k=0}^{\infty}\int_0^t (a_3(t-p) - a_3(\psi_6 + a_4)f_2(t-p)) \\ & \cdot \left(2L'\left(\frac{2k+1}{\sqrt{\psi_5}}, -\psi_6, p\right)\right) dp. \end{aligned} \tag{49}$$

Nusselt numbers

$$Nu_0 = -\frac{k_{nf}}{k_f}\frac{\partial \theta}{\partial y}\bigg|_{y=0} = -\frac{k_{nf}}{k_f} L^{-1}\left\{\frac{\partial \bar{\theta}}{\partial y}\bigg|_{y=0}\right\}. \tag{50}$$

By using equation (36) in equation (50),

$$Nu_0 = \frac{k_{nf}}{k_f}\left[\theta_1(t) - H(t-1)\theta_1(t-1)\right], \tag{51}$$

where

$$\begin{aligned} \theta_1(t) = {} & \frac{1}{\sqrt{\psi_5}}\sum_{k=0}^{\infty}\int_0^t \left(\frac{(t-p)^{1-\xi}}{\Gamma(2-\xi)} - \psi_6(t-p)\right) \\ & \cdot \left(L'\left(\frac{k}{\sqrt{\psi_5}}, -\psi_6, p\right) + L'\left(\frac{k+1}{\sqrt{\psi_5}}, -\psi_6, p\right)\right) dp, \end{aligned} \tag{52}$$

$$Nu_1 = -\frac{k_{nf}}{k_f}\frac{\partial \theta}{\partial y}\bigg|_{y=1} = -\frac{k_{nf}}{k_f} L^{-1}\left\{\frac{\partial \bar{\theta}}{\partial y}\bigg|_{y=1}\right\}, \tag{53}$$

By using equation (36) in equation (53),

$$Nu_1 = \frac{k_{nf}}{k_f}\left[\theta_2(t) - H(t-1)\theta_2(t-1)\right], \tag{54}$$

where

$$\theta_2(t) = \frac{1}{\sqrt{\psi_5}} \sum_{k=0}^{\infty} \int_0^t \left(\frac{(t-p)^{1-\xi}}{\Gamma(2-\xi)} - \psi_6(t-p) \right) \cdot \left(2L' \left(\frac{2k+1}{\sqrt{\psi_5}}, -\psi_6, p \right) \right) dp, \tag{55}$$

$$Sh_0 = -\frac{D_{nf}}{D_f} \frac{\partial C}{\partial y}\bigg|_{y=0} = -\frac{D_{nf}}{D_f} L^{-1} \left\{ \frac{\partial \bar{C}}{\partial y}\bigg|_{y=0} \right\}. \tag{56}$$

By using equation (29) in equation (56),

$$Sh_0 = \frac{D_{nf}}{D_f} [C_1(t) - H(t-1) C_1(t-1)], \tag{57}$$

where

$$C_1(t) = \frac{1}{\sqrt{\psi_7}} \sum_{k=0}^{\infty} \int_0^t \left(\frac{(t-p)^{1-\xi}}{\Gamma(2-\xi)} + \psi_8(t-p) \right) \cdot \left(L' \left(\frac{k}{\sqrt{\psi_7}}, \psi_8, p \right) + L' \left(\frac{k+1}{\sqrt{\psi_7}}, \psi_8, p \right) \right) dp, \tag{58}$$

$$Sh_1 = -\frac{D_{nf}}{D_f} \frac{\partial C}{\partial y}\bigg|_{y=1} = -\frac{D_{nf}}{D_f} L^{-1} \left\{ \frac{\partial \bar{C}}{\partial y}\bigg|_{y=1} \right\}. \tag{59}$$

By using equation (29) in equation (59),

$$Sh_1 = \frac{D_{nf}}{D_f} [C_2(t) - H(t-1) C_2(t-1)], \tag{60}$$

where

$$C_2(t) = \frac{1}{\sqrt{\psi_7}} \sum_{k=0}^{\infty} \int_0^t \left(\frac{(t-p)^{1-\xi}}{\Gamma(2-\xi)} + \psi_8(t-p) \right) \cdot \left(2L' \left(\frac{2k+1}{\sqrt{\psi_7}}, \psi_8, p \right) \right) dp. \tag{61}$$

3.5. Solution of Problem for Isothermal Conditions. For isothermal conditions equation (20) becomes $\theta(0,t) = C(0,t) = 1$, $u(0,t) = 0$.

$$C(y,t) = \sum_{k=0}^{\infty} \int_0^t \left(\frac{(t-p)^{-\xi}}{\Gamma(1-\xi)} + \psi_8 \right) \left(g \left(\frac{2k+y}{\sqrt{\psi_7}}, \psi_8, p \right) - g \left(\frac{2k+2-y}{\sqrt{\psi_7}}, \psi_8, p \right) \right) dp,$$

$$\theta(y,t) = \sum_{k=0}^{\infty} \int_0^t \left(\frac{(t-p)^{-\xi}}{\Gamma(1-\xi)} - \psi_6 \right) \left(g \left(\frac{2k+y}{\sqrt{\psi_5}}, -\psi_6, p \right) - g \left(\frac{2k+2-y}{\sqrt{\psi_5}}, -\psi_6, p \right) \right) dp,$$

$$u(y,t) = \sum_{k=0}^{\infty} \int_0^t \left((a_1 + a_3) + \frac{a_1(\psi_4 - a_2)}{a_2} f_3(t-p) + \frac{a_3(\psi_4 - a_4)}{a_4} f_4(t-p) \right) \left(g \left(\frac{2k+y}{\sqrt{\psi_1}}, \psi_4, p \right) - g \left(\frac{2k+2-y}{\sqrt{\psi_1}}, \psi_4, p \right) \right) dp - \sum_{k=0}^{\infty} \int_0^t \left(a_1 + \frac{a_1(\psi_8 - a_2)}{a_2} f_3(t-p) \right) \cdot \left(g \left(\frac{2k+y}{\sqrt{\psi_7}}, \psi_8, p \right) - g \left(\frac{2k+2-y}{\sqrt{\psi_7}}, \psi_8, p \right) \right) dp - \sum_{k=0}^{\infty} \int_0^t \left(a_3 - \frac{a_3(\psi_6 + a_4)}{a_4} f_4(t-p) \right) \cdot \left(g \left(\frac{2k+y}{\sqrt{\psi_5}}, -\psi_6, p \right) - g \left(\frac{2k+2-y}{\sqrt{\psi_5}}, -\psi_6, p \right) \right) dp, \tag{62}$$

where

$$f_3(t) = a_2 t^{\xi} E_{\xi,\xi+1}\left(-a_2 w^{\xi}\right), \qquad f_3(t) = a_4 t^{\xi} E_{\xi,\xi+1}\left(-a_4 w^{\xi}\right). \tag{63}$$

3.6. Sherwood Numbers, Skin Friction, and Nusselt Numbers (for Isothermal). Skin friction at $y = 0$ is defined as

$$C_{f_0} = \frac{1}{(1-\phi)^{2.5} \sqrt{\psi_1}} \sum_{k=0}^{\infty} \int_0^t \left((a_1 + a_3) + \frac{a_1(\psi_4 - a_2)}{a_2} f_3(t-p) + \frac{a_3(\psi_4 - a_4)}{a_4} f_4(t-p) \right) \left(L' \left(\frac{k}{\sqrt{\psi_1}}, \psi_4, p \right) + L' \left(\frac{k+1}{\sqrt{\psi_1}}, \psi_4, p \right) \right) dp - \frac{1}{(1-\phi)^{2.5} \sqrt{\psi_7}} \cdot \sum_{k=0}^{\infty} \int_0^t \left(a_1 + \frac{a_1(\psi_8 - a_2)}{a_2} f_3(t-p) \right) \cdot \left(L' \left(\frac{k}{\sqrt{\psi_7}}, \psi_8, p \right) + L' \left(\frac{k+1}{\sqrt{\psi_7}}, \psi_8, p \right) \right) dp - \frac{1}{(1-\phi)^{2.5} \sqrt{\psi_5}} \sum_{k=0}^{\infty} \int_0^t \left(a_3 - \frac{a_3(\psi_6 + a_4)}{a_4} f_4(t-p) \right) \cdot \left(L' \left(\frac{k}{\sqrt{\psi_5}}, -\psi_6, p \right) + L' \left(\frac{k+1}{\sqrt{\psi_5}}, -\psi_6, p \right) \right) dp. \tag{64}$$

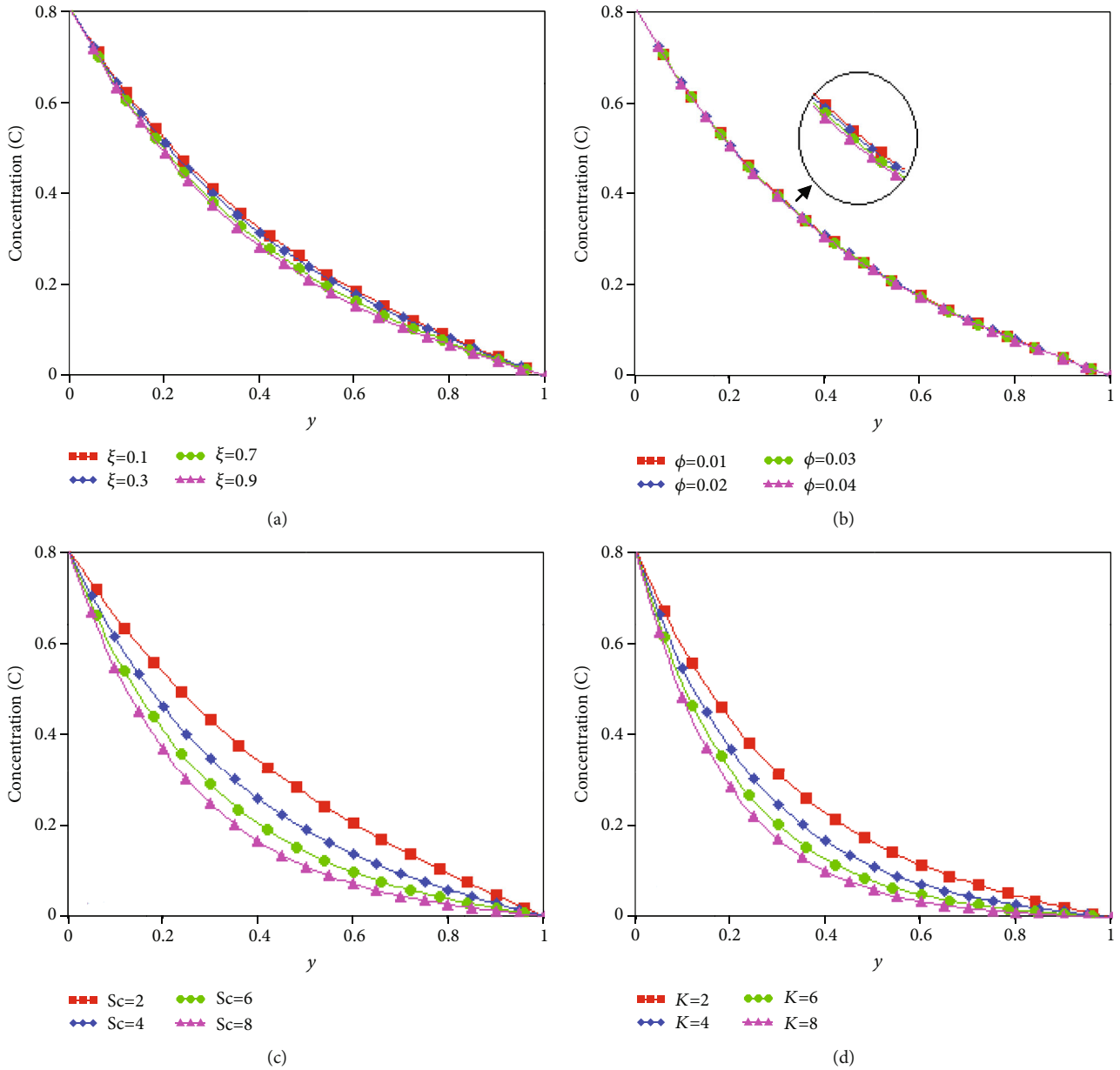

Figure 2: Variation of concentration.

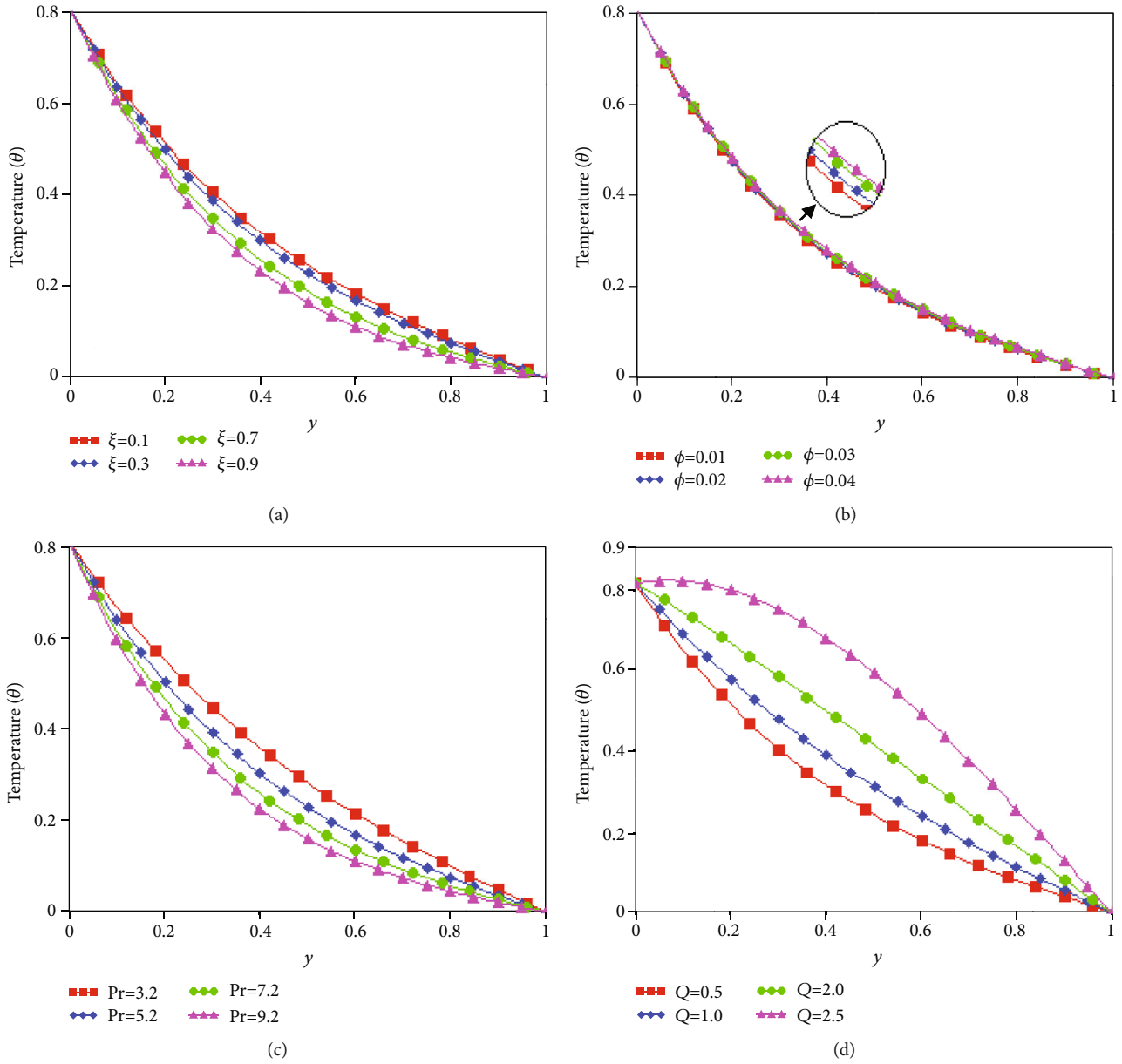

Figure 3: Variation of temperature.

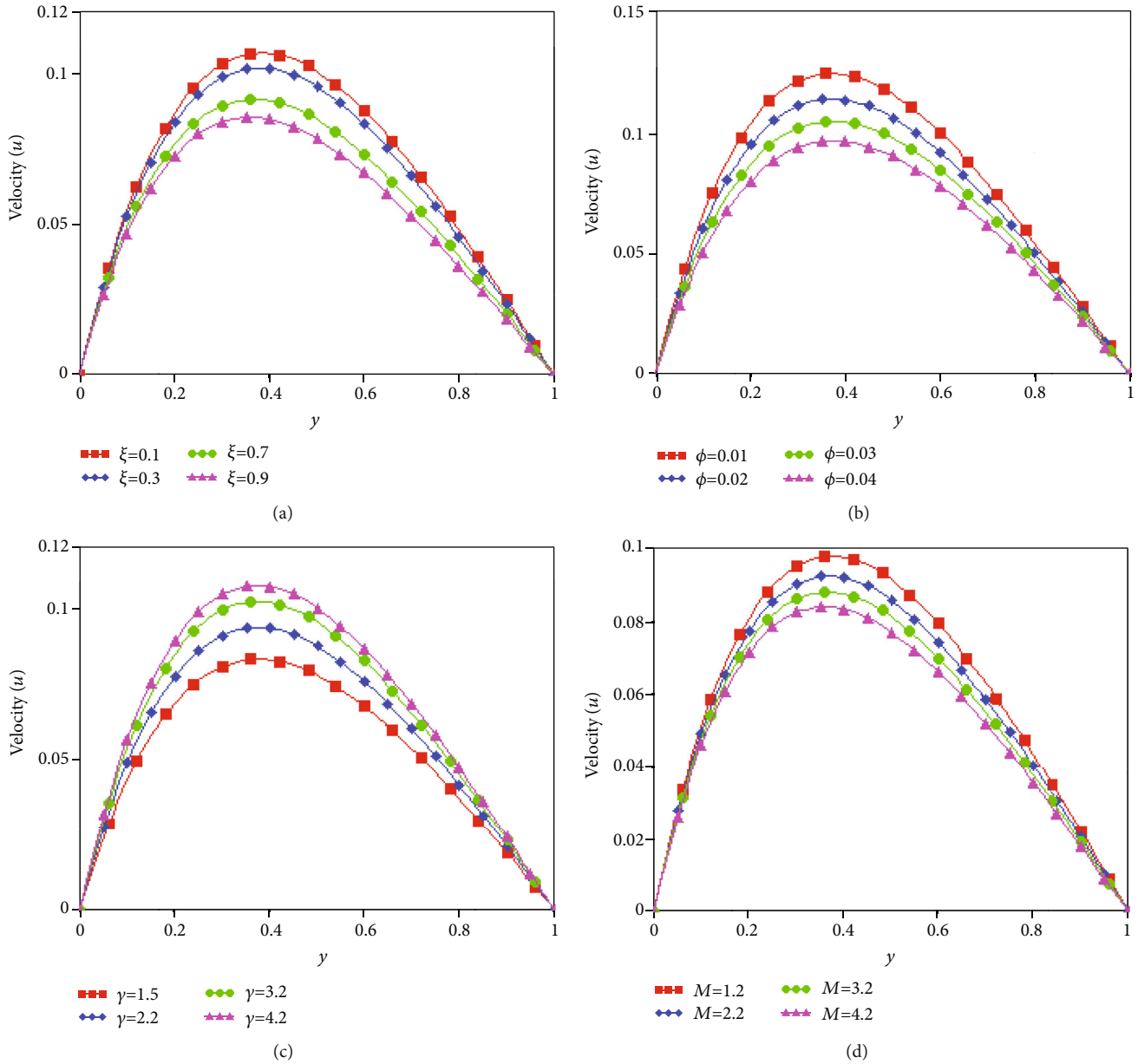

Figure 4: Continued.

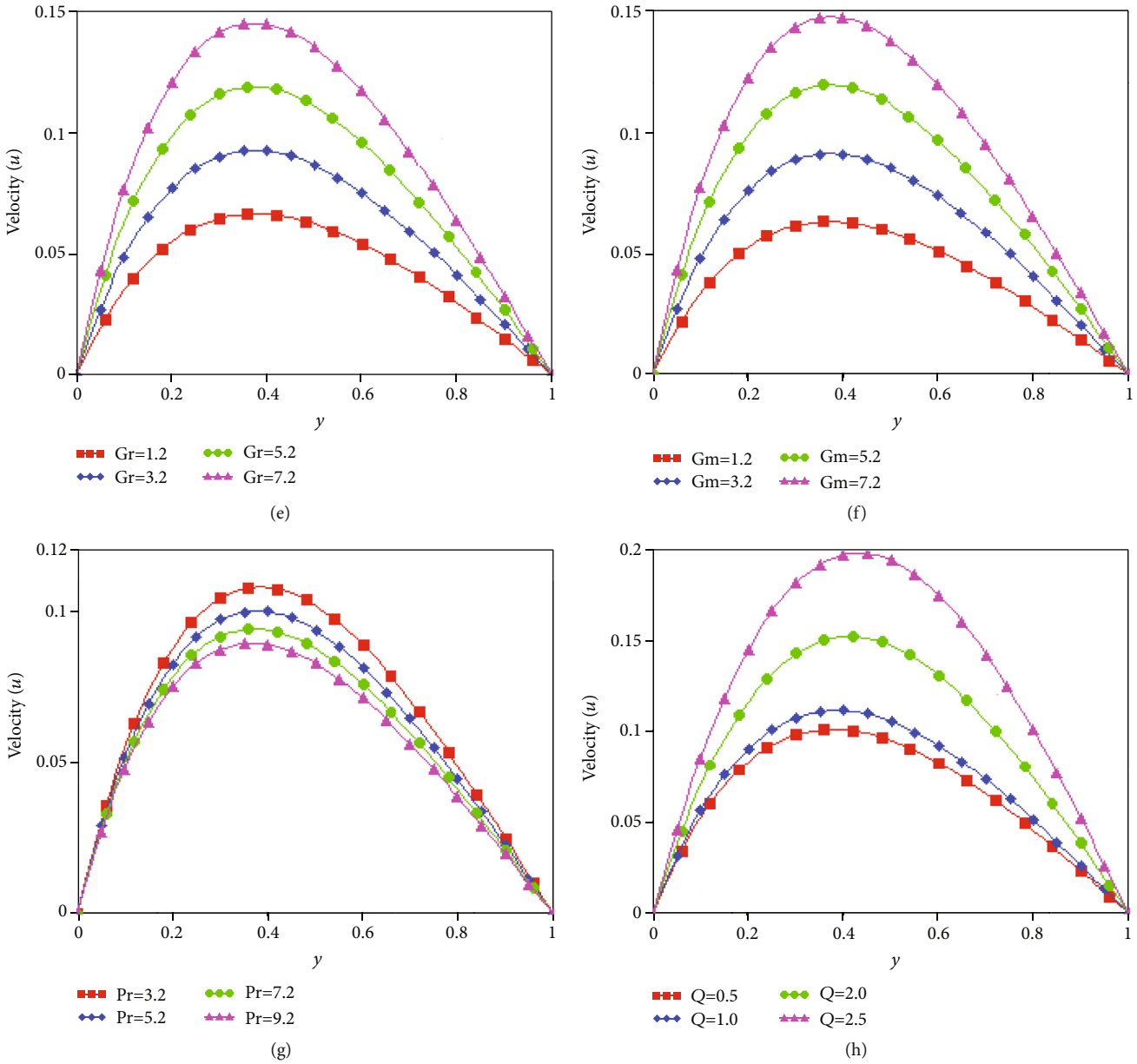

Figure 4: Continued.

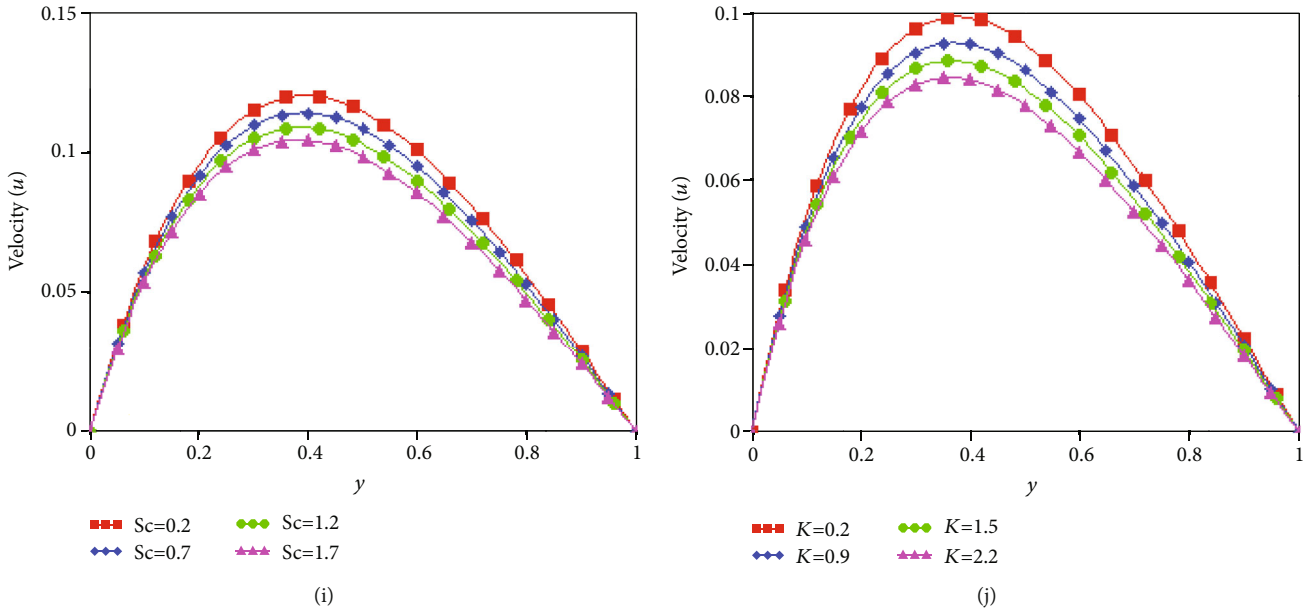

FIGURE 4: Variation of velocity.

Skin friction at $y = 1$ is defined as

$$C_{f_1} = \frac{1}{(1-\phi)^{2.5}\sqrt{\psi_1}}\sum_{k=0}^{\infty}\int_0^t\left((a_1+a_3)+\frac{a_1(\psi_4-a_2)}{a_2}f_3(t-p)+\frac{a_3(\psi_4-a_4)}{a_4}f_4(t-p)\right)\left(2L'\left(\frac{2k+1}{\sqrt{\psi_1}},\psi_4,p\right)\right)dp - \frac{1}{(1-\phi)^{2.5}\sqrt{\psi_7}}\sum_{k=0}^{\infty}\int_0^t\left(a_1+\frac{a_1(\psi_8-a_2)}{a_2}f_3(t-p)\right)\cdot\left(2L'\left(\frac{2k+1}{\sqrt{\psi_7}},\psi_8,p\right)\right)dp - \frac{1}{(1-\phi)^{2.5}\sqrt{\psi_5}}\cdot\sum_{k=0}^{\infty}\int_0^t\left(a_3-\frac{a_3(\psi_6+a_4)}{a_4}f_4(t-p)\right)\cdot\left(2L'\left(\frac{2k+1}{\sqrt{\psi_5}},-\psi_6,p\right)\right)dp. \tag{65}$$

Nusselt numbers

$$Nu_0 = \frac{1}{\sqrt{\psi_5}}\frac{k_{nf}}{k_f}\sum_{k=0}^{\infty}\int_0^t\left(\frac{(t-p)^{-\xi}}{\Gamma(1-\xi)}-\psi_6\right)\cdot\left(L'\left(\frac{k}{\sqrt{\psi_5}},-\psi_6,p\right)+L'\left(\frac{k+1}{\sqrt{\psi_5}},-\psi_6,p\right)\right)dp,$$

$$Nu_1 = \frac{1}{\sqrt{\psi_5}}\frac{k_{nf}}{k_f}\sum_{k=0}^{\infty}\int_0^t\left(\frac{(t-p)^{-\xi}}{\Gamma(1-\xi)}-\psi_6\right)\cdot\left(2L'\left(\frac{2k+1}{\sqrt{\psi_5}},-\psi_6,p\right)\right)dp. \tag{66}$$

Sherwood numbers

$$Sh_0 = \frac{1-\phi}{\sqrt{\psi_7}}\sum_{k=0}^{\infty}\int_0^t\left(\frac{(t-p)^{-\xi}}{\Gamma(1-\xi)}+\psi_8\right)\cdot\left(L'\left(\frac{k}{\sqrt{\psi_7}},\psi_8,p\right)+L'\left(\frac{k+1}{\sqrt{\psi_7}},\psi_8,p\right)\right)dp,$$

$$Sh_1 = \frac{1-\phi}{\sqrt{\psi_7}}\sum_{k=0}^{\infty}\int_0^t\left(\frac{(t-p)^{-\xi}}{\Gamma(1-\xi)}+\psi_8\right)\left(2L'\left(\frac{2k+1}{\sqrt{\psi_7}},\psi_8,p\right)\right)dp. \tag{67}$$

4. Graphical Results and Discussions

In this section, the influences of dimensionless parameters on fluid flow are discussed. The impact of ramped temperature, ramped concentration and volume fraction, and fractional and physical parameters on Casson nanofluid in a channel is analyzed.

For comparison, the graphs of nondimensional concentration, temperature, and velocity profiles corresponding to Casson parameter (γ), magnetic parameter (M), nanoparticle volume parameter (ϕ), Grashof numbers (Gr and Gr), Schmidt number (Sc), Prandtl number (Pr), heat generation (Q), chemical reaction (K), and fractional parameters (ξ) are shown in Figures 2–4. In the entire comparison all Casson parameter, $\gamma = 2.5$, $\phi = 0.04$, $\xi = 0.5$, $t = 0.8$, Pr = 6.2, $Gm = 3.6$, $Gr = 3.5$, $Q = 0.2$, $M = 1.5$, and $K = 0.5$ are fixed except the deviation in the respective figures.

Figures 2(a), 3(a), and 4(a) show the influence of ξ on concentration, temperature, and velocity fields. Velocity, concentration, and temperature obtained with derivatives are the better choice to have controlled results. The concentration, temperature, and velocity profiles reduce for higher values of ξ with ramped boundary conditions. Figures 2(b),

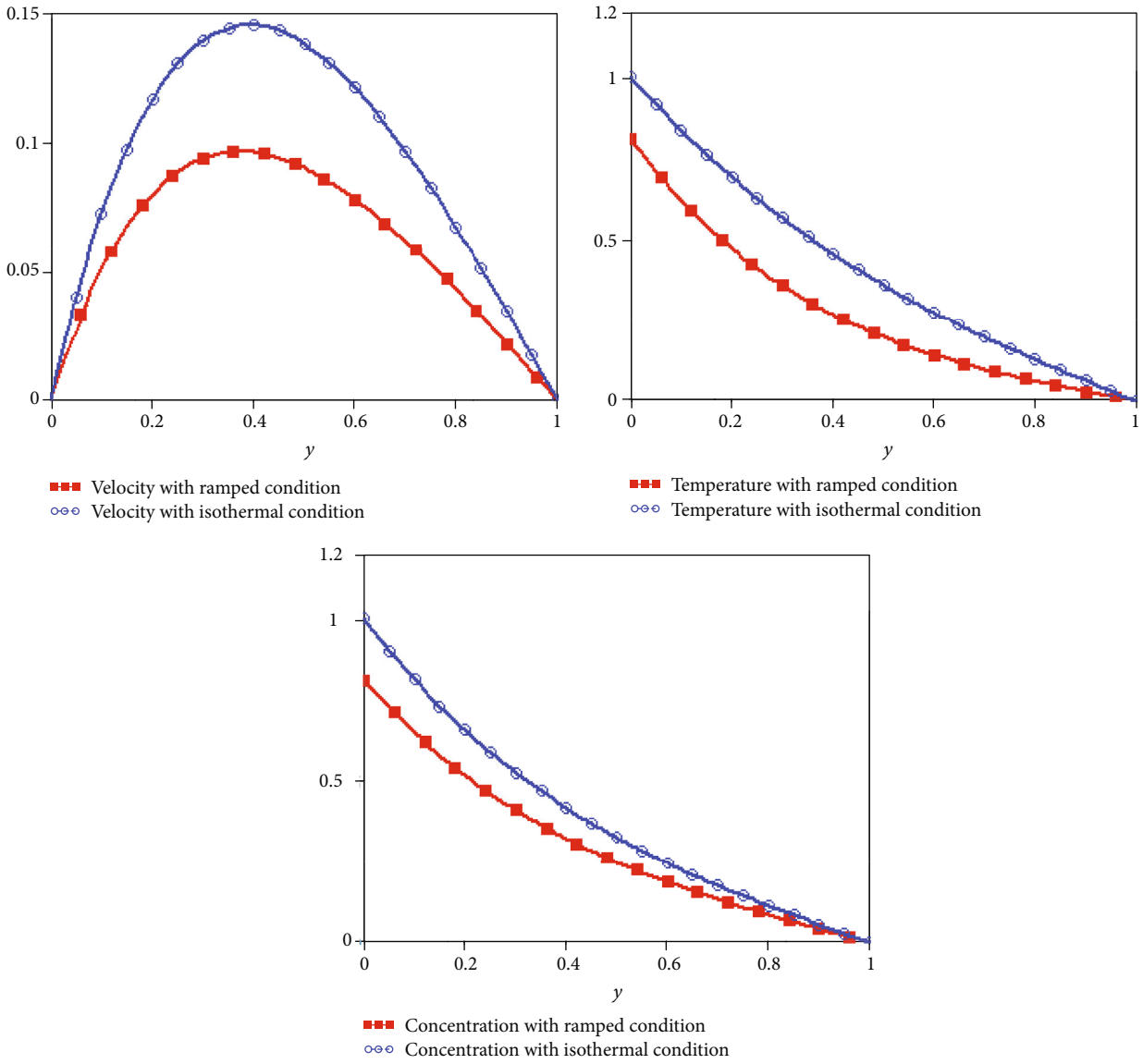

Figure 5: Comparison for velocity, temperature, and concentration fields with isothermal and ramped conditions.

3(b), and 4(b) depict the influence of ϕ on concentration, temperature, and velocity profiles. From Figures 2(b) and 4(b), it is noticed that the concentration and velocity of nanofluid decreases for higher values of ϕ. The increasing values of ϕ enhance the thickness and dynamic viscosity that reduce concentration and velocity of the nanofluid. Figure 3(b) illustrates that the temperature field of nanofluid increases due to the collision of nanoparticles for greater values of volume fraction. Also, the temperature increases due to the higher thermal conductivity of Cu nanoparticles.

Figures 2(c) and 4(i) demonstrate that the rise in Sc is similar to a poor solute diffusion which lets shallower dispersion of solute outcome. Consequently, the concentration and velocity reduce. Thus, the larger of Sc reduces the thickness of the boundary layer. Figures 2(d) and 4(g) indicate that the concentration and velocity fields reduce rapidly as K increases. The solute molecules increase under the influence of chemical reaction parameter.

Figures 3(c) and 4(g) show the impact of Pr on temperature and velocity. The higher values of Pr increase the viscosity of the nanofluid and reduce the heat transport rate of the nanofluid that reduces velocity and temperature. Figures 3(d) and 4(h) illustrate that by increasing $Q > 0$, the heat is discharged due to which temperature and velocity increase.

Figure 4(c) demonstrates the impact of the Casson parameter on velocity. The flow increases by increasing γ. Figure 4(d) reflects the influence of magnetic parameter (M) on the velocity field. An increase in M reduces the

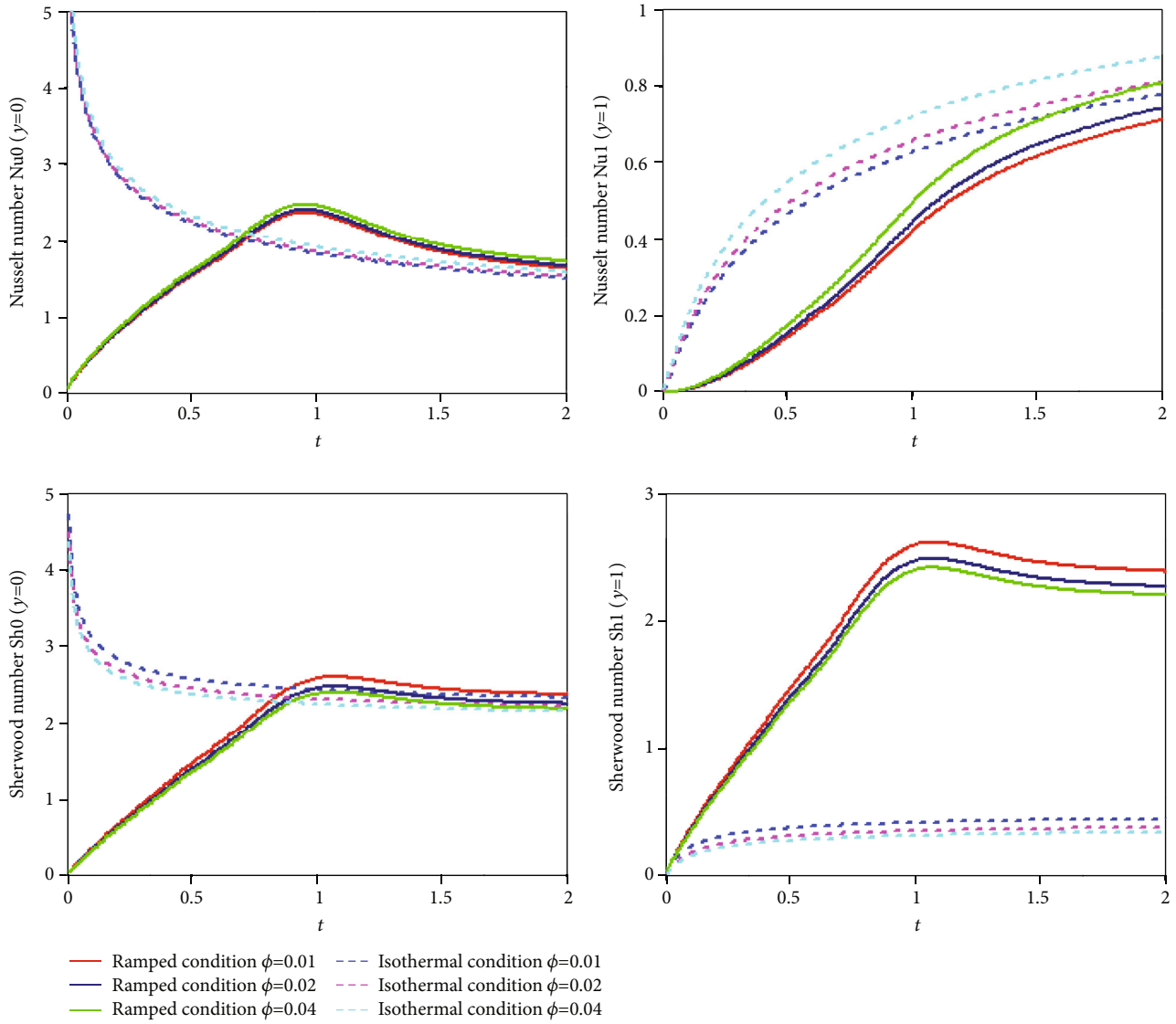

Figure 6: Effects of ϕ on Nusselt and Sherwood numbers.

thickness of the flow boundary and decreases the velocity. Figures 4(e) and 4(f) show that the velocity increases for increasing Grashof numbers (Gr and Gm). Grashof numbers indicate the relative significance of viscous force to buoyancy force. The viscous effect in velocity reduces by large Grashof numbers.

Figure 5 illustrates the comparison of velocity, concentration, and temperature with constant and ramped boundary conditions. It established that ramped velocity, concentration, and temperature are lower than acquired by isothermal conditions. Thus, the ramped boundary conditions are more stable.

Figure 6 shows the variations in Nusstle and Sherwood numbers on both plates with ramped and isothermal conditions. The Sherwood numbers decrease and Nusselt numbers increase by increasing volume fraction.

Figure 7 illustrates the comparison of present results with existing results of Ramzan et al. [31]. It is concluded that in the absence of ϕ, porosity and Dufour effects the results are identical.

5. Conclusions

An unsteady Casson nanofluid flow within a channel with ramped concentration and temperature is investigated. Furthermore, chemical reaction, heat generation, and magnetic effects are considered. The problem is generalized by Caputo time-fractional derivative, and Laplace transform is used to find analytical results of ramped and isothermal boundary conditions. In this work, SA is considered as a base fluid containing the nanoparticles of Cu. The significant results for velocity, concentration, temperature, Nusselt numbers,

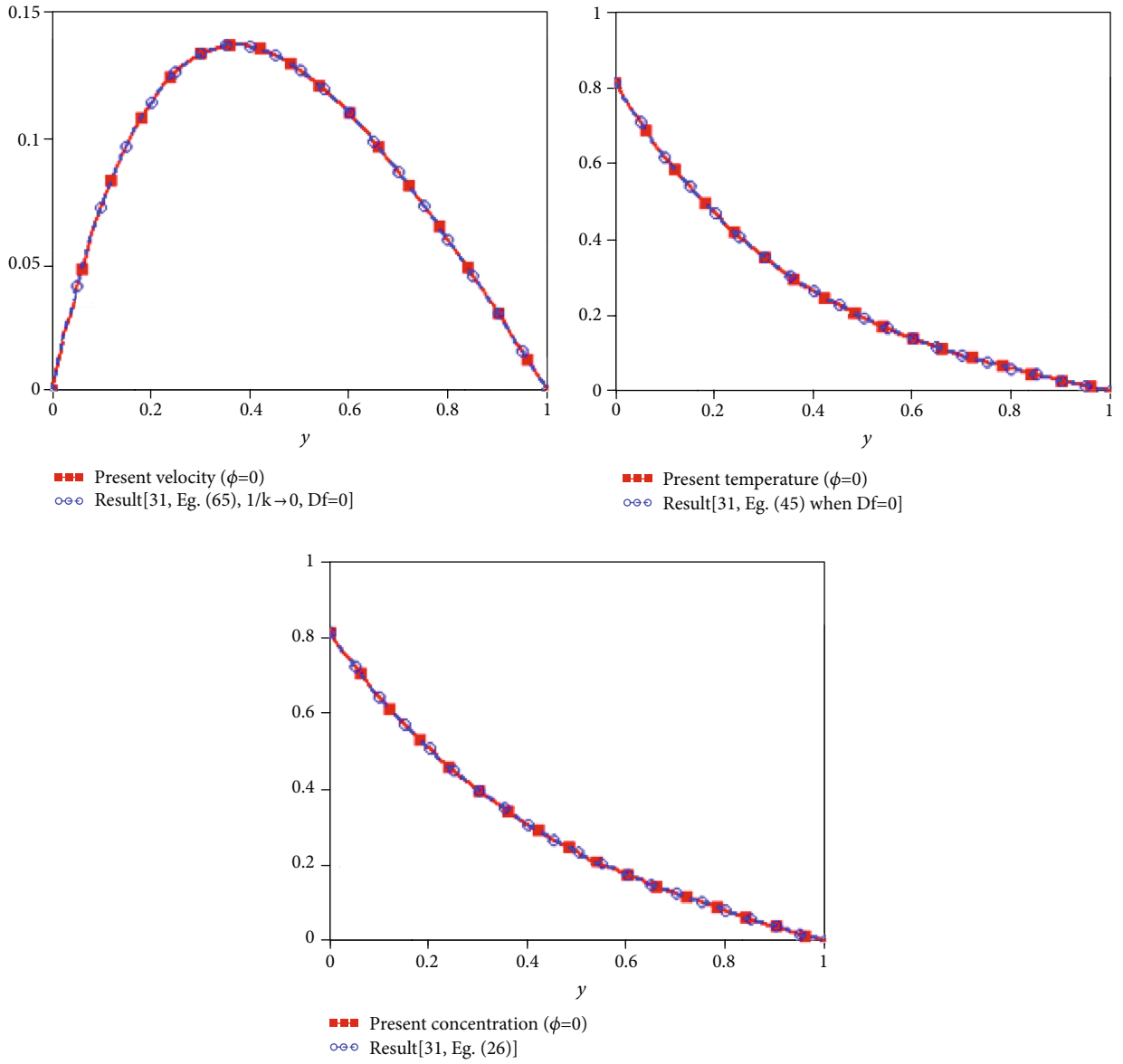

Figure 7: Comparison of results.

and Sherwood numbers are graphically underlined and discussed in detail.

The major points of this work are as follows:

(i) Velocity, concentration, and temperature are lesser for ramped boundary conditions than isothermal

(ii) Ramped wall velocity is increasing for greater values of γ, Gr, Gm, and Q and decreasing for higher values of ξ, ϕ, M, Pr, Sc, and K

(iii) Ramped wall temperature is decreasing for higher values of ξ and Pr and decreasing for growing values of ϕ and Q

(iv) Ramped wall concentration is decreasing for increasing values of ξ, ϕ, Sc, and K

(v) Sherwood and Nusselt numbers both are increasing function of ϕ for both isothermal and ramped conditions

(vi) Velocity, concentration, and temperature obtained with ordinary derivatives are higher than that obtained by fractional derivatives. Thus, the fractional derivative is a better choice to have controlled results

(vii) Ramped boundary conditions are useful to manage velocity, concentration, and temperature profiles

Appendix

$$L^{-1}\left\{\frac{e^{-a\sqrt{s^{\xi}+b}}}{\sqrt{s^{\xi}+b}}\right\} = \int_0^{\infty} \frac{1}{\sqrt{\pi w}} e^{\left(-\frac{a^2}{4w}-bw\right)} t^{-1}\Phi\left(0,-\xi,-wt^{-\xi}\right) dw,$$

$$L^{-1}\left\{\frac{e^{-a\sqrt{s^{\xi}+b}}}{s^{\xi}+b}\right\} = \int_0^{\infty} e^{-bw}\ \mathrm{erfc}\left(\frac{a}{2\sqrt{w}}\right) t^{-1}\Phi\left(0,-\xi,-wt^{-\xi}\right) dw,$$

$$L^{-1}\left\{\frac{1}{\left(s^{\xi}+a\right)s^2}\right\} = \int_0^{t} w^{\xi-1} E_{\xi,\xi+1}\left(-aw^{\xi}\right) dw,$$

$$L^{-1}\left\{\frac{a}{\left(s^{\xi}+a\right)s}\right\} = at^{\xi} E_{\xi,\xi+1}\left(-aw^{\xi}\right),$$

$$L^{-1}\left\{\frac{1}{s^{\xi}}\right\} = \frac{t^{\xi-1}}{\Gamma(\xi)}. \tag{A1}$$

Nomenclature

$\tilde{u}(\tilde{y},\tilde{t})$: Velocity ($\mathrm{m\,s^{-1}}$)
$\tilde{C}(\tilde{y},\tilde{t})$: Concentration ($\mathrm{kg\,m^{-3}}$)
$\tilde{T}(\tilde{y},\tilde{t})$: Temperature (K)
Q_0: Heat generation coefficient ($\mathrm{W\ m^{-3}\ K^{-1}}$)
k: Thermal conductivity ($\mathrm{W\ m^{-1}\ K^{-1}}$)
g: Gravitational acceleration ($\mathrm{m\ s^{-2}}$)
Q: Dimensionless heat generation
D: Mass diffusivity ($\mathrm{m^2\,s^{-1}}$)
R: Chemical reaction coefficient ($\mathrm{s^{-1}}$)
Gm: Mass Grashof number
c_p: Specific heat ($\mathrm{J\ kg^{-1}\ K^{-1}}$)
K: Dimensionless chemical reaction
Gr: Thermal Grashof number
Sc: Schmidt number
Pr: Prandtl number
C_f: Skin friction
Sh: Sherwood number
Nu: Nusselt number.

Greek Symbols

γ: Casson parameter
ρ: Density ($\mathrm{kg\ m^{-3}}$)
β_C: Mass volumetric coefficient ($\mathrm{m^3\,kg^{-1}}$)
ν: Kinematic viscosity (m2 s-1)
β_T: Thermal expansion coefficient ($\mathrm{K^{-1}}$)
θ: Dimensionless temperature
μ: Dynamic viscosity ($\mathrm{kg\ m^{-1}\ s^{-1}}$)
ϕ: Nanoparticle volume fraction
σ: Electric conductivity $(\Omega\mathrm{m})^{-1}$.

Subscript

nf: Fluid
nf: Nanofluid
s: Solid particles.

Data Availability

No data were used in this manuscript.

Conflicts of Interest

The authors declare that they have no conflicts of interest.

Acknowledgments

The author Rifaqat Ali would like to express his gratitude to the Deanship of Scientific Research at King Khalid University, Saudi Arabia, for providing funding research groups under the research grant no. R. G. P. 1/162/42.

References

[1] N. Casson, *A Flow Equation for Pigment-Oil Suspensions of the Printing Ink Type, Rheology of Disperse Systems*, Pergamon Press, London, UK, 1959.

[2] R. K. Dash, K. N. Mehta, and G. Jayaraman, "Casson fluid flow in a pipe filled with a homogenous porous medium," *International Journal of Engineering Science*, vol. 34, no. 10, pp. 1145–1156, 1996.

[3] M. Usman, T. Gul, A. Khan, A. Alsubie, and M. Z. Ullah, "Electromagnetic couple stress film flow of hybrid nanofluid over an unsteady rotating disc," *International Communications in Heat and Mass Transfer*, vol. 127, article 105562, 2021.

[4] A. Saeed, M. Jawad, W. Alghamdi, S. Nasir, T. Gul, and P. kumam, "Hybrid nanofluid flow through a spinning Darcy-Forchheimer porous space with thermal radiation," *Scientific Reports*, vol. 11, no. 1, article 16708, 2021.

[5] M. Bilal, A. Saeed, M. M. Selim, T. Gul, I. Ali, and P. Kumam, "Comparative numerical analysis of Maxwell's time-dependent thermo-diffusive flow through a stretching cylinder," *Case Studies in Thermal Engineering*, vol. 27, article 101301, 2021.

[6] A. Saeed, W. Alghamdi, S. Mukhtar et al., "Darcy-Forchheimer hybrid nanofluid flow over a stretching curved surface with heat and mass transfer," *PLoS One*, vol. 16, no. 5, article e0249434, 2021.

[7] I. Zari, A. Shafiq, G. Rasool, T. N. Sindhu, and T. S. Khan, "Double-stratified Marangoni boundary layer flow of Casson nanoliquid: probable error application," *Journal of Thermal Analysis and Calorimetry*, 2021.

[8] B. Ali, G. Rasool, S. Hussain, D. Baleanu, and S. Bano, "Finite element study of magnetohydrodynamics (MHD) and activation energy in Darcy–Forchheimer rotating flow of Casson Carreau nanofluid," *PRO*, vol. 8, no. 9, p. 1185, 2020.

[9] A. Shafiq, G. Rasool, H. Alotaibi et al., "Thermally enhanced Darcy-Forchheimer Casson-water/glycerine rotating nanofluid flow with uniform magnetic field," *Micromachines*, vol. 12, no. 6, p. 605, 2021.

[10] A. A. Hayday, D. A. Bowlus, and R. A. McGraw, "Free convection from a vertical flat plate with step discontinuities in surface temperature," *Journal of Heat Transfer*, vol. 89, no. 3, pp. 244–249, 1967.

[11] J. A. Schetz, "On the approximate solution of viscous-flow problems," *Journal of Applied Mechanics*, vol. 30, no. 2, pp. 263–268, 1963.

[12] C. P. Malhotra, R. L. Mahajan, W. S. Sampath, K. L. Barth, and R. A. Enzenroth, "Control of temperature uniformity during the manufacture of stable thin-film photovoltaic devices," *International Journal of Heat and Mass Transfer*, vol. 49, no. 17–18, pp. 2840–2850, 2006.

[13] R. McIntosh and S. Waldram, "Obtaining more, and better, information from simple ramped temperature screening tests," *Journal of Thermal Analysis and Calorimetry*, vol. 73, no. 1, pp. 35–52, 2003.

[14] S. Das, M. Jana, and R. N. Jana, "Radiation effect on natural convection near a vertical plate embedded in porous medium with ramped wall temperature," *Open Journal of Fluid Dynamics*, vol. 1, no. 1, pp. 1–11, 2011.

[15] R. Nandkeolyar, M. Das, and P. Sibanda, "Exact solutions of unsteady MHD free convection in a heat absorbing fluid flow past a flat plate with ramped wall temperature," *Boundary Value Problems*, vol. 2013, no. 1, 2013.

[16] G. S. Seth, S. M. Hussain, and S. Sarkar, "Hydromagnetic natural convection flow with heat and mass transfer of a chemically reacting and heat absorbing fluid past an accelerated moving vertical plate with ramped temperature and ramped surface concentration through a porous medium," *Journal of the Egyptian Mathematical Society*, vol. 23, no. 1, pp. 197–207, 2015.

[17] G. S. Seth, R. Sharma, and S. Sarkar, "Natural convection heat and mass transfer flow with hall current, rotation, radiation and heat absorption past an accelerated moving vertical plate with ramped temperature," *Journal of Applied Fluid Mechanics*, vol. 8, no. 1, pp. 7–20, 2015.

[18] G. S. Seth, S. Sarkar, S. M. Hussain, and G. K. Mahato, "Effects of hall current and rotation on hydromagnetic natural convection flow with heat and mass transfer of a heat absorbing fluid past an impulsively moving vertical plate with ramped temperature," *Journal of Applied Fluid Mechanics*, vol. 8, no. 1, pp. 159–171, 2015.

[19] G. S. Seth, M. S. Ansari, and R. Nandkeolyar, "MHD natural convection flow with radiative heat transfer past an impulsively moving plate with ramped wall temperature," *Heat and Mass Transfer*, vol. 47, no. 5, pp. 551–561, 2011.

[20] N. A. Mohd Zin, I. Khan, and S. Shafie, "Influence of thermal radiation on unsteady MHD free convection flow of Jeffrey fluid over a vertical plate with ramped wall temperature," *Mathematical Problems in Engineering*, vol. 2016, 12 pages, 2016.

[21] M. Narahari, "Transient free convection flow between long vertical parallel plates with ramped wall temperature at one boundary in the presence of thermal radiation and constant mass diffusion," *Meccanica*, vol. 47, no. 8, pp. 1961–1976, 2012.

[22] A. Khalid, I. Khan, and S. Shafie, "Exact solutions for free convection flow of nanofluids with ramped wall temperature," *European Physical Journal Plus*, vol. 130, no. 4, p. 4, 2015.

[23] B. Mahanthesh, B. J. Gireesha, and R. S. R. Gorla, "Heat and mass transfer effects on the mixed convective flow of chemically reacting nanofluid past a moving/stationary vertical plate," *Alexandria Engineering Journal*, vol. 55, no. 1, pp. 569–581, 2016.

[24] B. K. Jha and Y. Y. Gambo, "Soret and Dufour effects on transient free convention heat and mass transfer flow in a vertical channel with ramped wall temperature and specie concentration: an analytical approach," *Arab Journal of Basic and Applied Sciences*, vol. 27, no. 1, pp. 344–357, 2020.

[25] M. Arif, P. Kumam, W. Kumam, I. Khan, and M. Ramzan, "A fractional model of Casson fluid with ramped wall temperature: engineering applications of engine oil," *Computational and Mathematical Methods*, no. article e1162, 2021.

[26] T. Anwar, P. Kumam, I. Khan, and W. Watthayu, "Heat transfer enhancement in unsteady MHD natural convective flow of CNTs Oldroyd-B nanofluid under ramped wall velocity and ramped wall temperature," *Entropy*, vol. 22, no. 4, p. 401, 2020.

[27] C. Li, D. Qian, and Y. Chen, "On Riemann-Liouville and caputo derivatives," *Discrete Dynamics in Nature and Society*, vol. 2011, 15 pages, 2011.

[28] N. Heymans and I. Podlubny, "Physical interpretation of initial conditions for fractional differential equations with Riemann-Liouville fractional derivatives," *Rheologica Acta*, vol. 45, no. 5, pp. 765–771, 2006.

[29] M. Turkyilmazoglu, "Exact analytical solutions for heat and mass transfer of MHD slip flow in nanofluids," *Chemical Engineering Science*, vol. 84, pp. 182–187, 2012.

[30] M. Hatami and D. D. Ganji, "Natural convection of sodium alginate (SA) non-Newtonian nanofluid flow between two vertical flat plates by analytical and numerical methods," *Case Studies in Thermal Engineering*, vol. 2, pp. 14–22, 2014.

[31] M. Ramzan, M. Nazar, Z. Un Nisa, M. Ahmad, and N. Ali Shah, "Unsteady free convective magnetohydrodynamics flow of a Casson fluid through a channel with double diffusion and ramp temperature and concentration," *Mathemtical Methods in Applied Sciences*, pp. 1–20, 2021.

[32] I. Siddique, K. Sadiq, I. Khan, and K. S. Nisar, "Nanomaterials in convection flow of nanofluid in upright channel with gradients," *Journal of Materials Research and Technology*, vol. 11, pp. 1411–1423, 2021.

[33] S. Kakaç and A. Pramuanjaroenkij, "Review of convective heat transfer enhancement with nanofluids," *International Journal of Heat and Mass Transfer*, vol. 52, no. 13-14, pp. 3187–3196, 2009.

[34] H. F. Oztop and E. Abu-Nada, "Numerical study of natural convection in partially heated rectangular enclosures filled with nanofluids," *International Journal of Heat and Fluid flow*, vol. 29, no. 5, pp. 1326–1336, 2008.